

# High-performance 90° hybrid based on a silicon-on-insulator multimode interference coupler

R. Halir,<sup>1,\*</sup> G. Roelkens,<sup>2</sup> A. Ortega-Moñux,<sup>1</sup> and J. G. Wangüemert-Pérez<sup>1</sup>

<sup>1</sup>Departamento Ingeniería de Comunicaciones, ETSI Telecomunicación, Universidad de Málaga, 29010 Málaga, Spain

<sup>2</sup>Department of Information Technology (INTEC), Ghent University—Interuniversity Microelectronics Center (IMEC), B-9000 Gent, Belgium

\*Corresponding author: robert.halir@ic.uma.es

Received October 27, 2010; revised December 7, 2010; accepted December 7, 2010; posted December 8, 2010 (Doc. ID 137252); published January 10, 2011

We propose a multimode interference coupler (MMI) design for high-index-contrast technologies based on a shallowly etched multimode region, which is, for the first time to our knowledge, directly coupled to deeply etched input and output waveguides. This reduces the phase errors associated with the high-index contrast, while still allowing for a very compact layout. Using this structure, we fabricate a  $2 \times 4$  MMI operating as a 90° hybrid, with a footprint of only  $0.65 \text{ mm} \times 0.53 \text{ mm}$ , including all the structures necessary to couple light to a fiber array. We experimentally demonstrate a common mode rejection ratio better than  $-20 \text{ dB}$  and phase errors better than  $\pm 5^\circ$  in a  $\sim 50 \text{ nm}$  bandwidth. © 2011 Optical Society of America

OCIS codes: 130.3120, 230.7370.

Multimode interference couplers (MMIs) are widely used devices in integrated optics, because they provide large bandwidth and relaxed fabrication tolerances. Applications include Mach–Zehnder interferometers [1], resonators [2], and 90° hybrids for coherent optical receivers [3–5]. The latter enable optical-fiber-based long-haul transmissions with drastic increases in data rates without sacrificing additional bandwidth by using complex quadrature and phase modulations such as quaternary phase shift keying. High-index-contrast technologies, such as silicon-on-insulator (SOI) and deeply etched indium phosphide (InP) are attractive platforms for the implementation of such components, because they allow for very compact designs and small waveguide curvature radii, which allow for complex interconnections. Practical receivers furthermore require polarization management and power detection. In SOI, the former may be achieved, for example, via polarization diversity using polarization splitting fiber-to-chip grating couplers [6], and the latter with hybrid integration or germanium photodetectors [7].

However, the high-index contrast of deeply etched InP and SOI platforms hinders the design of high-performance MMIs, as explained as follows. The basic operation of MMIs consists in launching light from one of the access waveguides (numbered 1 and 2 in Fig. 1), into the wide multimode section where it expands into multiple modes. These travel with different propagation constants and, at certain imaging distances, interfere to form replicas of the input field, which are coupled to the output waveguides (numbered 3 to 6 in Fig. 1). The formation of these images is governed by the self-imaging theory [8], which essentially requires that all the modes excited in the multimode section exhibit quadratically related propagation constants, i.e.,

$$\beta_m = \beta_1 - (m^2 - 1)\pi/(3L_\pi), \quad (1)$$

where  $m = 1, 2, 3, \dots$  is the mode number and  $L_\pi$  is the beat length of the two lowest order modes. In waveguides with high-lateral ( $x$  direction)-index contrast, such as

deeply etched InP ridges and silicon wires, this relation between the propagation constants holds only for the lower-order modes, resulting in strong phase errors for the higher-order modes [9]. These phase errors result in low-quality imaging, and they become especially detrimental as the number of MMI inputs or outputs grows.

A number of techniques have been proposed to overcome this problem. First, by increasing the access waveguide width, only the lowest-order modes, which exhibit almost ideal propagation constants, are excited [10–12]. This requires careful design of the access waveguide width, because increasing it too much results in unnecessarily large devices [10]. Second, using shallowly etched waveguides [9] reduces the index contrast, thus alleviating the phase error. However, this yields larger devices, because the shallowly etched input and output waveguides need to be further separated to avoid coupling between them, and sacrifices the small curvature radii. Finally, simulations of MMIs with engineered, quasi-optimum refractive index profile in the multimode region show compact, high-performance devices [13]. Yet the engineered refractive index profile is difficult to implement.

Here we propose an MMI design, operating as a 90° hybrid, that achieves good imaging quality while maintaining compactness typical for high index contrast technology. Using silicon wire technology, we demonstrate, for the first time to our knowledge, the use of a shallowly etched multimode region coupled directly to deeply etched waveguides that exhibit tight curvature radii and allow a dense spacing. Experimental results confirm the excellent performance of the device.

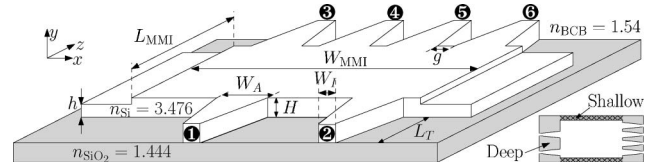


Fig. 1. Schematic drawing of the proposed MMI geometry. Refractive indices are given at  $\lambda = 1.55 \mu\text{m}$ .

The proposed design is shown in Fig. 1. The silicon core layer is  $H = 220$  nm thick, and the single-mode interconnecting waveguides are  $W_I = 0.45$   $\mu\text{m}$  wide. The minimum gap between the output waveguides is set to  $g = 0.5$   $\mu\text{m}$  to avoid coupling between them, and DVS-BCB (divinyl siloxane bis-benzocyclobutene) is used as the cladding material. The access waveguides are completely etched, but the multimode region is etched only to a depth of  $D = H - h$  to reduce the index contrast.

To determine the optimum etch depth of the multimode region, we calculated the propagation constants of its TE polarized modes for a fixed width  $W_{\text{MMI}} = 7.7$   $\mu\text{m}$ , using the commercial FimmWave mode solver. The deviation of the simulated propagation constants from their ideal distribution defined by (1) was then computed. Multiplying this deviation by the fourfold imaging distance,  $(3/8)L_{\pi}$ , gives the accumulated phase error for each mode. This error is plotted in Fig. 2 for different heights ( $h$ ) of the lateral slab. From Fig. 2 it is clear that a fully etched ( $h = 0$  nm) multimode region yields very large, negative phase errors. Reducing the etch depth, i.e., increasing  $h$ , reduces the maximum possible propagation angle in the multimode region, but it also drastically reduces the phase error of the modes that remain guided. Reducing the etch depth below 70 nm ( $h > 150$  nm) again produces increased, positive phase errors. Thus, the etch depth was fixed at 70 nm ( $h = 150$  nm), which also makes the fabrication of the devices compatible with the definition of the fiber-to-chip grating couplers, which are etched 70 nm deep into the silicon waveguide layer [14].

Despite using a shallowly etched multimode region, here we propose the use of fully etched access waveguides. While this may seem counterintuitive, it has several advantages. First, it reduces coupling between the output waveguides, so they can be placed closer together, reducing the footprint of the device. Second, it obviates the need of a transition between the fully etched interconnecting waveguides and the shallowly etched multimode region. Finally, it enables the use of tight bends in the input and output waveguides. In [10], it was shown that low-loss coupling of the access waveguides requires that the input mode profile exhibit the same symmetry in the vertical direction as the modes supported by the multimode region. Figure 3 shows that, as expected, the mode field of the input waveguide is virtually symmetric in the vertical direction. The mode

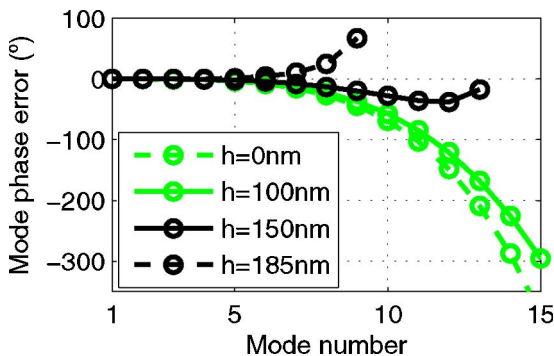


Fig. 2. (Color online) Mode phase error as a function of mode propagation angle for different heights of the lateral slab ( $h$ ).

fields of the multimode region, despite being shallowly etched, exhibit the same type of symmetry, with the exception of the edge of the device, where the field is distorted, owing to the presence of the lateral slab. Because the input and output waveguides are not placed at the edge of the multimode region, low-loss coupling is feasible. However, because of the reduced-index contrast, the multimode region supports only a limited number of modes. Consequently, the input waveguide width has to be designed such that only the guided modes are excited. Eigenmode expansion simulations with the commercial FimmProp package show that a waveguide width of  $W_A = 1.5$   $\mu\text{m}$  ensures that at least 98% of the incident power couples into guided modes of the multimode region. An approximately 10- $\mu\text{m}$ -long linear taper provides an adiabatic transition between the interconnecting waveguides ( $W_I = 0.45$   $\mu\text{m}$ ) and the MMI access waveguides ( $W_A = 1.5$   $\mu\text{m}$ ). The width ( $W_{\text{MMI}}$ ) and length ( $L_{\text{MMI}}$ ) of the multimode region were iteratively optimized to yield minimum imbalance and insertion losses. The resulting dimensions are  $W_{\text{MMI}} = 7.7$   $\mu\text{m}$  and  $L_{\text{MMI}} = 115.5$   $\mu\text{m}$ .

For testing purposes, TE-polarized light is coupled in and out of the chip with grating couplers. To facilitate accurate characterization, the  $2 \times 4$  MMI was embedded into the following test structure. The light coupled into the chip is divided by a  $1 \times 2$  MMI. One of the  $1 \times 2$  MMI outputs is fed directly into input 1 of the  $2 \times 4$  MMI, whereas light from the other output travels through a delay line before entering input 2 of the  $2 \times 4$  MMI. When scanning the input wavelength, this delay creates an interferogram at each of the  $2 \times 4$  MMI outputs from which its amplitude and phase characteristics can be obtained [15]. The input and output gratings were aligned so that they are accessible with a fiber array, enabling simultaneous detection of the four outputs. The complete test structure occupies an area of  $0.65$  mm  $\times$   $0.53$  mm, which is essentially determined by the 127  $\mu\text{m}$  spacing of the fibers in the array.

The device was fabricated within the ePIXfab network [16], on an SOI wafer with a silicon thickness of 220 nm. Structures were defined with deep UV lithography and a two etch depth process. A 70 nm etch was used for the

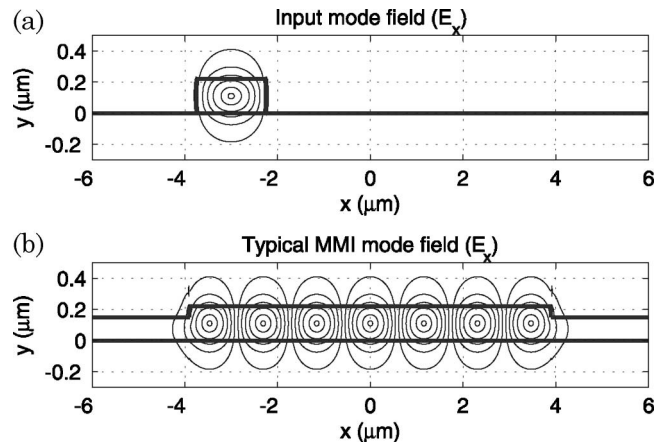


Fig. 3. Mode field of (a) the fully etched access waveguide and of (b) one of the modes of the shallowly etched multimode region.

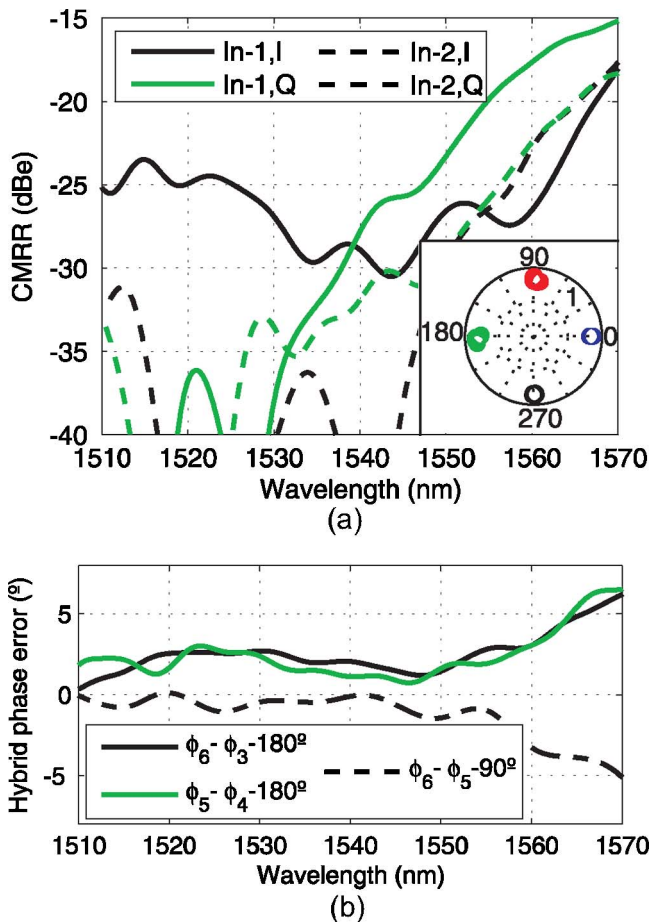


Fig. 4. (Color online) (a) CMRR of the fabricated device as a function of wavelength. (b) Phase error between the hybrid outputs as a function of wavelength.

multimode region and the grating couplers, whereas the photonic wires were fully etched.

The performance of a  $90^\circ$  hybrid is often quantified in terms of the common mode rejection ratio (CMRR) and phase error. Denoting by  $p_i$  the power at each output, the CMRR for the in-phase channel is defined as  $\text{CMRR}[\text{dBe}] = 20 \log_{10}[(p_3 - p_6)/(p_3 + p_6)]$ , when power is launched from either input [the CMRR is measured in electrical decibels (dBes), hence the factor 20]. For the quadrature channel  $p_3$  and  $p_6$  are substituted by  $p_4$  and  $p_5$ , respectively. Defining  $\phi_i$  as the relative phase with which waves from inputs 1 and 2 combine at outputs  $i = 3, \dots, 6$ , the relevant phase errors of the hybrid are  $\phi_6 - \phi_3 - 180^\circ$ ,  $\phi_5 - \phi_4 - 180^\circ$ , and  $\phi_6 - \phi_5 - 90^\circ$ . Figure 4(a) shows the measured CMRR of the device in the 1500 nm–1560 nm band, which is well below  $-20$  dBe in a 45 nm bandwidth. The phase error is within  $\pm 5^\circ$  in a 55 nm bandwidth [see Fig. 4(b)]. The device thus readily matches the performance of state-of-the-art  $90^\circ$

hybrids, which have footprint up to 20 times larger [4,5]. The inset in Fig. 4(a) shows the relative amplitudes and phases with which the hybrid combines the waves from the two inputs at each output.

We have proposed and demonstrated an MMI design for high-index-contrast platforms, based on a shallowly etched multimode region to reduce the modal phase error, and deeply etched access waveguides to allow for a compact overall layout. A  $90^\circ$  hybrid based on this design exhibits excellent performance and an ultracompact footprint. While the concept is demonstrated here in silicon technology, it is directly applicable to other platforms, such as deeply etched InP.

This work was supported by the Spanish Ministerio de Ciencia (project TEC2009-10152), a Formación del Profesorado Universitario scholarship (AP-2006-03355), and by the Andalusian Regional Ministry of Science (project TIC-02946).

## References

1. D. Kim, A. Barkai, R. Jones, N. Elek, H. Nguyen, and A. Liu, *Opt. Lett.* **33**, 530 (2008).
2. D.-X. Xu, A. Densmore, P. Waldron, J. Lapointe, E. Post, A. Delâge, S. Janz, P. Cheben, J. Schmid, and B. Lamontagne, *Opt. Express* **15**, 3149 (2007).
3. T. Niemeier and R. Ulrich, *Opt. Lett.* **11**, 677 (1986).
4. S. Jeong and K. Morito, *Opt. Express* **18**, 4275 (2010).
5. H.-G. Bach, A. Matiss, C. Leonhardt, R. Kunkel, D. Schmidt, M. Schell, and A. Umbach, in *Optical Fiber Communication Conference*, OSA Technical Digest (CD) (Optical Society of America, 2009), paper OMK5.
6. Y. Tang, D. Dai, and S. He, *IEEE Photon. Technol. Lett.* **21**, 242 (2009).
7. S. Assefa, F. Xia, and Y. A. Vlasov, *Nature* **464**, 80 (2010).
8. M. Bachmann, P. Besse, and H. Melchior, *Appl. Opt.* **33**, 3905 (1994).
9. J. Huang, R. Scarmozzino, and R. Osgood, *IEEE Photon. Technol. Lett.* **10**, 1292 (1998).
10. R. Halir, I. Molina-Fernández, A. Ortega-Moñux, J. G. Wangüemert-Pérez, D.-X. Xu, P. Cheben, and S. Janz, *J. Lightwave Technol.* **26**, 2928 (2008).
11. D. J. Thomson, Y. Hu, G. T. Reed, and J.-M. Fedeli, *IEEE Photon. Technol. Lett.* **22**, 1485 (2010).
12. A. Hosseini, H. Subbaraman, D. Kwong, Y. Zhang, and R. T. Chen, *Opt. Lett.* **35**, 2864 (2010).
13. I. Molina-Fernández, A. Ortega-Moñux, and J. G. Wangüemert-Pérez, *J. Lightwave Technol.* **27**, 1307 (2009).
14. G. Roelkens, D. Vermeulen, F. V. Laere, S. Selvaraja, S. Scheerlinck, D. Taillaert, W. Bogaerts, P. Dumon, D. V. Thourhout, and R. Baets, *J. Nanosci. Nanotechnol.* **10**, 1551 (2010).
15. R. Halir, A. Ortega-Moñux, I. Molina-Fernández, J. G. Wangüemert-Pérez, P. Cheben, D.-X. Xu, B. Lamontagne, and S. Janz, *J. Lightwave Technol.* **27**, 5405 (2009).
16. Available at: <http://www.epixfab.eu>.